*electronics*

MDPI

*Article*

# A Multireceiver Wireless Power Supply System with Power Equalization in Stereoscopic Space

**Bin Shi [1], Feng Wen [2,*] and Xiaohu Chu [2]**

[1] School of Electrical Engineering, Southeast University, Nanjing 210096, China; 101005279@seu.edu.cn
[2] School of Automation, Nanjing University of Science and Technology, Nanjing 210094, China; chu@njust.edu.cn
* Correspondence: wen@njust.edu.cn; Tel.: +86-159-9620-0950

**Abstract:** With the rapid development of wireless power transfer (WPT) technology, the traditional single-transceiver WPT system has become more and more advanced; however, it is still difficult to meet its extensive application requirements. Aiming at the wireless charging of mobile phones in public places, electric vehicles (EVs) in multistorey garages, and electronic shelf labels (ESLs) in supermarket merchandise shelves, a multireceiver wireless power supply system with power equalization is proposed. The condition of power equalization is derived according to the equivalent circuit of the proposed WPT system, and the received power can be equally maintained by adjusting the transceiver loop resistance when the total load number or transmission distance changes. A simulation model is established to evaluate the electromagnetic environment of the proposed WPT system, and the results comply with the electromagnetic safety of the ICNIRP-2018 guidelines. Finally, the experimental results show that the power differential rate that meets the power equalization condition is 13 to 17% lower than that of the unsatisfied rate, which verifies the effectiveness of the proposed system in terms of power equalization.

**Keywords:** wireless power transfer (WPT); stereoscopic space; multireceivers; power equalization



**Citation:** Shi, B.; Wen, F.; Chu, X. A Multireceiver Wireless Power Supply System with Power Equalization in Stereoscopic Space. *Electronics* **2021**, *10*, 713. https://doi.org/10.3390/electronics10060713

Academic Editor: Pedro Pinho

Received: 21 February 2021
Accepted: 16 March 2021
Published: 18 March 2021



## 1. Introduction

In recent years, wireless power transfer (WPT) technology has attracted widespread attention and research due to its safe and convenient characteristics [1,2]. At present, the technology has been successfully used in consumer electronics, electric vehicles, implantable devices, etc., [3–5].

With the rapid development of WPT technology, the ordinary single-transceiver system has been relatively widespread, but it is still difficult to meet its wide application requirements [6]. For a multireceiver WPT system with loads, the distribution and control of received power is the focus of this research [7]. By designing a nonuniform gap thickness between the transmitter and the receiver at a specific location, the uniformity of the induced power of multiple receivers can be improved [8]. On the other hand, it is necessary to maximize system efficiency while meeting the power requirements of each load [9]. However, external factors, such as changes in transmission distance and load, may lead to the power received becoming unstable, which will cause great damage to the electrical equipment. To solve this problem, researchers have studied various techniques.

The series energy storage battery in the WPT system is designed with a voltage equalizer using a voltage multiplier, which can achieve single-switch voltage equalization without feedback control [10]. Based on the automatic frequency tracing technique, the problem of frequency shifts when the load number changes can be solved [11]. By periodically short-circuiting the receiver coil closest to the transmitter coil, the magnetic flux of the remote receiver coil can be controlled to equalize the received power among all receiver coils [12]. Auxiliary circuits, including band-pass and/or band-stop circuits, are proposed

to be incorporated into receiver circuits and optional relay circuits to facilitate the selection and enhancement of wireless power transmission to designated loads [13].

Efforts to improve the efficiency of multiple receivers are productive in the field of active equalizers, such as switched capacitors, converters based on the transformer, and so on [14,15]. Through the reconfigurable shape of the modular WPT array system, multiple power flow paths are provided in the space between the transmitter and the receiver, thereby improving the reliability of power transmission [16]. However, circuits using these components, or the various control techniques, usually have issues of complexity which will intensify further when more receivers are added in the WPT system [17].

At the same time, various standards for WPT technology have been released to standardize designs applied in different fields, from developers such as SAE J2954-(R) for EVs [18] and Qi standard for mobile devices [19]. Moreover, electromagnetic radiation around the WPT system cannot be ignored during the working period. As such, the International Commission on Non-Ionizing Radiation Protection (ICNIRP), the American National Standards Institute (ANSI), and the Institute of Electrical and Electronics Engineers (IEEE) worked on many standards to give a reference to limit magnetics, such as the ICNIRP-2010 Guidelines, the ICNIRP-2018 Guidelines, IEEE Std C95.3$^{TM}$-2002, IEEE Std C95.1$^{TM}$-2005, etc., [20–23].

In this paper, we propose a stereoscopic space wireless power transfer (WPT) system, and present a method by adjusting the loop resistances of transmitter and relay transmitter coils to satisfy the condition of power equalization under different transmission distances or load numbers. The proposed method is more efficient, convenient, and economic in keeping power equalization of all loads in stereoscopic space, especially when there exist many loads. Only the resistances of transmitter and relay transmitter coils are adjusted to achieve power equalization, instead of redesigning all receiver coils. A simulation model is built to study the H-field intensity around the WPT system compared with the ICNIRP-2018 guidelines. Furthermore, experimental verification is also carried out to validate the feasibility of the proposed scheme.

## 2. Proposed Structure and Power Equalization

A block diagram of this paper is shown in Figure 1.

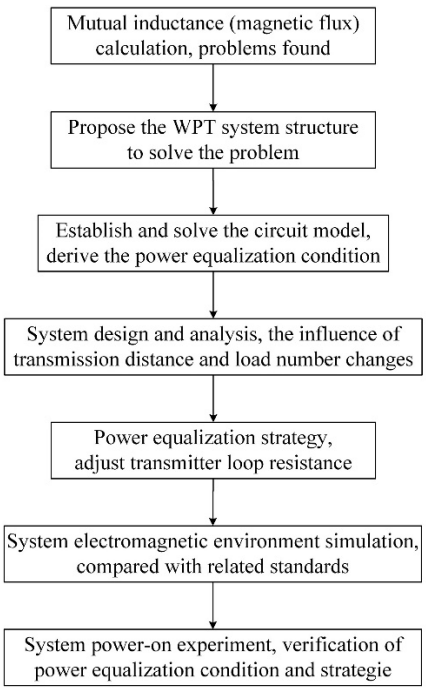


**Figure 1.** The block diagram of this paper. WPT—wireless power transfer.

Planar spiral coils are widely used in wireless power transfer systems. In order to study the magnetic flux of receiver coils and the mutual inductance between transmitter and receiver coils, a theoretical calculation model is established, as shown in Figure 2, including single-turn transmitter and receiver coils.

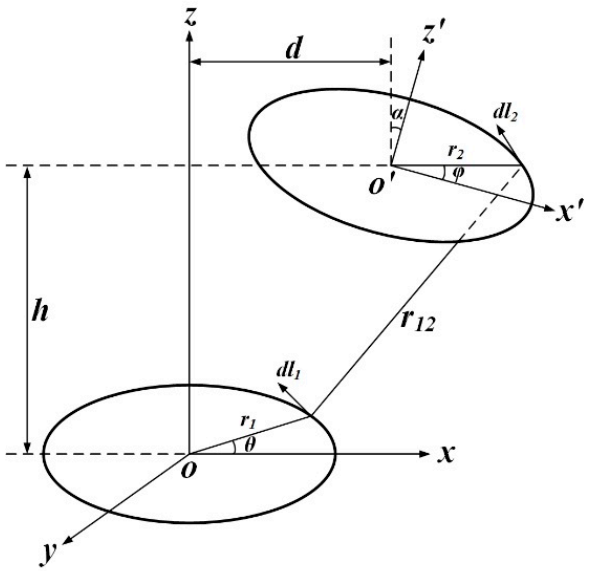


**Figure 2.** Single-turn transmitter and receiver coils at any spatial location.

According to the Niemann formula, the mutual inductance between two coils can be expressed as:

$$\begin{cases} M = \frac{\mu_0}{4\pi} \oint \oint \frac{dl_1 dl_2}{r_{12}} \\ dl_1 = r_1(-\sin\times\theta \vec{i} + \cos\theta \times \vec{j})d\theta \\ dl_2 = r_2(-\sin\varphi\cos\alpha \times \vec{i} + \cos\varphi \times \vec{j} + \sin\varphi\sin\alpha \times \vec{k})d\varphi \\ r_{12} = \sqrt{(x_1-x_2)^2+(y_1-y_2)^2+(z_1-z_2)^2} \\ \quad = [r_1^2 + r_2^2 + d^2 + h^2 + 2r_2 d\cos\varphi\cos\alpha - 2r_2 h\cos\varphi\sin\alpha \\ \quad - 2r_1 d\cos\theta - 2r_1 r_2(\cos\theta\cos\varphi\cos\alpha + \sin\theta\sin\varphi)]^{\frac{1}{2}} \end{cases} \tag{1}$$

where $\mu_0$ is the vacuum permeability, $l_1$ and $l_2$ are the length of each turn, $dl_1$ and $dl_2$ are the infinitesimal of $l$, and $r_{12}$ is the distance of $dl_1$ and $dl_2$.

Then,

$$M = \frac{\mu_0 r_1 r_2}{4\pi}\int_0^{2\pi}\int_0^{2\pi}\frac{\sin\theta\sin\varphi\cos\alpha + \cos\theta\cos\varphi}{r_{12}}d\theta d\varphi \tag{2}$$

For the planar spiral coil:

$$M_P = \sum_{i=1}^{n_1}\sum_{j=1}^{n_2} M_{ij} \tag{3}$$

Assuming that the transmitter current is $I_{TX}$, the magnetic flux on the receiver coil can be obtained by the following formula:

$$\Phi_S = M_P \times I_{TX} \tag{4}$$

By setting parameter values reasonably, the relationship between magnetic flux $\Phi$ and transmission distance $h$ can be obtained according to (3) and (4).

As shown in Figure 3, $\Phi$ will decrease sharply when $h$ increases, so it is challenging to sustain enough output power for receiver coils at different heights simultaneously, unless input current is added to increase the input power, which will contribute to the high power

supplied by the front-end driver and cause potential safety hazards. More often, it is difficult to put into practice.

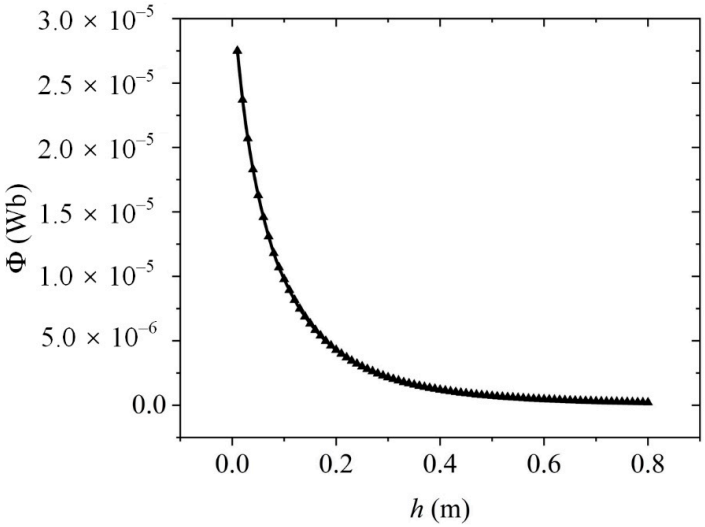


**Figure 3.** Relationship between the transmission distance $h$ and the magnetic flux Φ.

To solve the problem mentioned above, a new type of WPT system, with multiple receiver coils at different layers in stereoscopic space, is proposed. The proposed structure diagram is shown in Figure 4. TX1 represents the transmitter coil, while TX2 to TXk represent the relay transmitter coils of each layer. Receiver coils, RX, are symmetrically placed on TX. All RXs will acquire the same transmission power by configuring corresponding parameters properly.

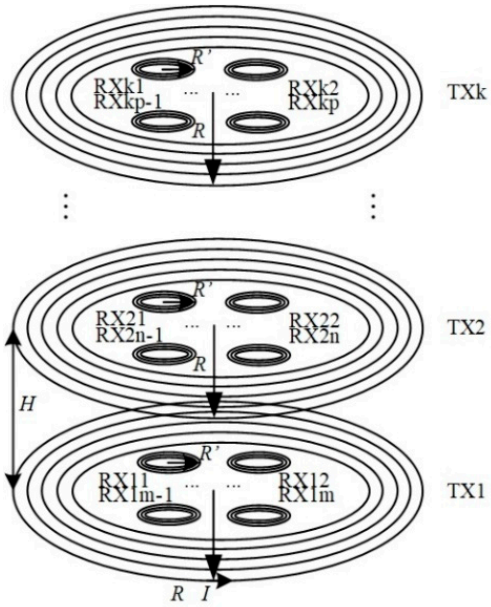


**Figure 4.** The structure of the proposed WPT system.

According to the coupling mechanism of the stereoscopic space wireless power transfer system with multilayers, the corresponding equivalent circuit diagram can be obtained, as shown in Figure 5.

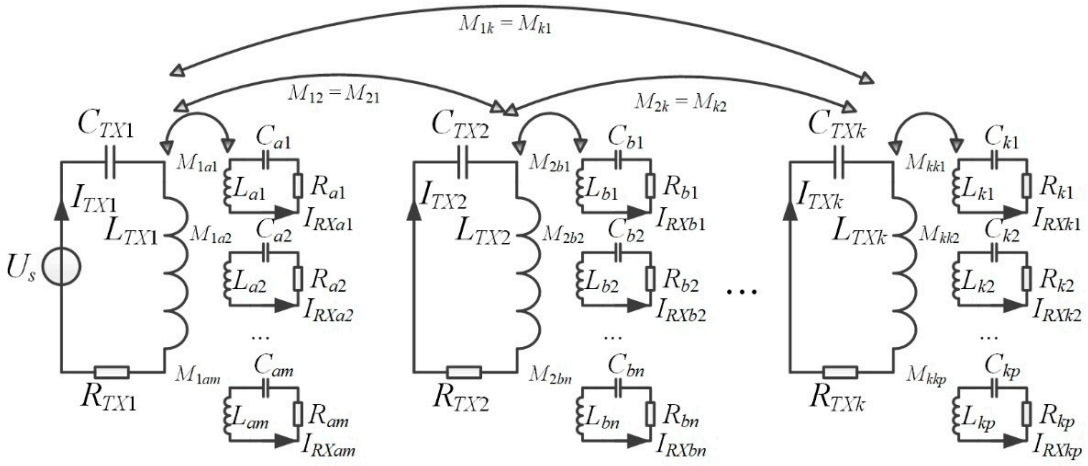


**Figure 5.** The equivalent circuit of the proposed WPT system.

The Kirchhoff Voltage Laws (KVL) equations for the first layer of the transmitter coil, for each layer of the relay transmitter coil, and for the receiver coils are listed, respectively, as follows:

$$\dot{U}=\begin{bmatrix}\dot{U}_S\\0\\\vdots\\0\\0\\\vdots\\0\end{bmatrix},Z=\begin{bmatrix}Z_{TX1}&j\omega M_{1a1}&\cdots&j\omega M_{1am}&j\omega M_{12}&\cdots&j\omega M_{1kp}\\j\omega M_{1a1}&Z_{11}&\cdots&j\omega M_{a1am}&j\omega M_{2a1}&\cdots&j\omega M_{a1kp}\\\vdots&\vdots&\ddots&\vdots&\vdots&\vdots&\vdots\\0&\cdots&j\omega M_{1am}&Z_{1m}&j\omega M_{2am}&\cdots&j\omega M_{amkp}\\j\omega M_{12}&j\omega M_{2a1}&\cdots&j\omega M_{2am}&Z_{TX2}&\cdots&j\omega M_{2kp}\\\vdots&\vdots&\vdots&\vdots&\vdots&\ddots&\vdots\\j\omega M_{1kp}&j\omega M_{kpa1}&\cdots&j\omega M_{kpam}&j\omega M_{2kp}&\cdots&Z_{kp}\end{bmatrix},\dot{I}=\begin{bmatrix}\dot{I}_{TX1}\\\dot{I}_{RXa1}\\\vdots\\\dot{I}_{RXam}\\\dot{I}_{TX2}\\\vdots\\\dot{I}_{RXkp}\end{bmatrix} \quad (5)$$

$$\dot{U}=Z\cdot\dot{I},\quad Z_{TXk}=R_{TXk}+j\omega L_{TXk}+\frac{1}{j\omega C_{TXk}},\quad Z_{kp}=R_{kp}+j\omega L_{kp}+\frac{1}{j\omega C_{kp}}$$

where $U_s$ represents the input voltage; $\omega$ is the angular frequency; $I_{TXk}$ represents the current passing through TX of the $k$th layer; $I_{RXkp}$ represents the current in the $p$th RX of the $k$th layer; $R_{TXk}$, $L_{TXk}$ and $C_{TXk}$, respectively, represent the resistance, inductance and series resonant capacitance of the TX loop of the $k$th layer; $R_{kp}$, $L_{kp}$ and $C_{kp}$, respectively, represent the resistance, inductance and series resonant capacitance of $p$th RX loop of the $k$th layer; $M_{k(k-1)}$ represents mutual inductance between the $k$th layer and $(k-1)$th layer TX; and $M_{kkp}$ represents mutual inductance between the $k$th layer TX and $p$th RX of the same layer.

In fact, there are many mutual inductances in (5) that can be ignored, such as the mutual inductance between different RXs, the mutual inductance between TX and RX of different layers, etc. Thus, Z will be a sparse matrix, and, in Section 3 (Table 1), we will quantitatively calculate these mutual inductance values to show that they can be ignored.

**Table 1.** Coil parameters.

| Parameter | *N* | $D_{min}$ (cm) | $D_{max}$ (cm) | *D* (cm) | *L* (μH) | *M* (μH) |
|---|---|---|---|---|---|---|
| TX1 | 34 | 35.4 | 50.58 | 0.23 | 750.47 | $M_{12}=M_{21}=48$ |
| RX2 | 9 | 5 | 7.48 | 0.155 | 7.70 | $M_{1am}=M_{2bn}=3.76$ |
| TX1 | 34 | 35.4 | 50.58 | 0.23 | 750.47 | $M_{\mathrm{a1am}}=M_{\mathrm{b1bn}}=0.024$ |
| RX2 | 9 | 5 | 7.48 | 0.155 | 7.70 | $M_{1bn}=0.99$, $M_{2am}=1.15$ |

We can assume that the RXs of the same layer are identical and evenly distributed on the TX. The mutual inductance between each RX and TX is equal. Since all loops are

resonant, the currents in all RXs of each layer are also equal. Considering the first two layers and the first RX, the following equations can be obtained:

$$\begin{cases} \dot{U}_S = R_{TX1}\dot{I}_{TX1} + mj\omega M_{1a1}\dot{I}_{RX1} + j\omega M_{12}\dot{I}_{TX2} \\ 0 = j\omega M_{1a1}\dot{I}_{TX1} + R_{a1}\dot{I}_{RX1} \\ 0 = R_{TX2}\dot{I}_{TX2} + nj\omega M_{2b1}\dot{I}_{RX2} + j\omega M_{12}\dot{I}_{TX1} \\ 0 = j\omega M_{2b1}\dot{I}_{TX2} + R_{b1}\dot{I}_{RX2} \end{cases} \tag{6}$$

where $R_{TX1}$ and $R_{TX2}$ represent the resistance of the TX loop on the first and the second layer, $R_{a1}$ and $R_{b1}$ are the resistance of the first RX loop on the first and the second layer, $M_{1a1}$ represents mutual inductance between the first TX and the first RX on the first layer, while $M_{2b1}$ is mutual inductance between the second TX and the first RX on the second layer, $M_{12}$ represents mutual inductance between the first TX and the second TX, $m$ and $n$ are the total number of RX on the first layer and the second layer, respectively. $I_{TX1}$, $I_{TX2}$, $I_{RX1}$ and $I_{RX2}$ are the current in TX1, TX2, RX1, and RX2, respectively, which can be expressed by:

$$\begin{cases} \dot{I}_{TX1} = \dfrac{\dot{U}_s}{R_{TX1} + \frac{m\omega^2 M_{1a1}^2}{R_{a1}} + \frac{\omega^2 M_{12}^2}{R_{TX2} + \frac{n\omega^2 M_{2b1}^2}{R_{b1}}}} \\ \dot{I}_{TX2} = -\dfrac{j\omega M_{12}\dot{U}_s}{\left(R_{TX2} + \frac{n\omega^2 M_{2b1}^2}{R_{b1}}\right)\left(R_{TX1} + \frac{m\omega^2 M_{1a1}^2}{R_{a1}}\right) + \omega^2 M_{12}^2} \\ \dot{I}_{RX1} = -\dfrac{j\omega M_{1a1}\dot{U}_s}{R_{a1}R_{TX1} + m\omega^2 M_{1a1}^2 + \frac{R_{a1}\omega^2 M_{12}^2}{R_{TX2} + \frac{n\omega^2 M_{2b1}^2}{R_{b1}}}} \\ \dot{I}_{RX2} = -\dfrac{\omega^2 M_{2b1} M_{12}\dot{U}_s}{\left(R_{b1}R_{TX2} + n\omega^2 M_{2b1}^2\right)\left(R_{TX1} + \frac{m\omega^2 M_{1a1}^2}{R_{a1}}\right) + R_{b1}\omega^2 M_{12}^2} \end{cases} \tag{7}$$

The total output power of the WPT system $P$ and the transmission efficiency $\eta$ can be calculated by (8) and (9), respectively.

$$P = mI_{RX1}^2 R_{a1} + nI_{RX2}^2 R_{b1} \tag{8}$$

$$\eta = \frac{mI_{RX1}^2 R_{a1} + nI_{RX2}^2 R_{b1}}{U_s I_{TX1}} \tag{9}$$

In order to equalize $I_{RX1}$ and $I_{RX2}$, $M_{12}$ should satisfy:

$$M_{12} = \frac{R_{b1}M_{1a1}}{R_{a1}M_{2b1}}\left(\frac{R_{TX2}}{\omega} + \frac{n\omega M_{2b1}^2}{R_{b1}}\right) \tag{10}$$

We can also obtain that $I_{TX1} = I_{TX2}$ as (10) is valid. According to (3) and (10), we can distribute the RX if TX is determined, or the TX can be determined if RX is known. We will discuss this further in the next section.

## 3. System Design and Analysis

The size parameters of the WPT system were designed according to the actual size of mobile phone wireless chargers, as shown in Table 1, where $N$ represents the turn number of TX or RX, $D_{min}$ and $D_{max}$ are the inner diameter and outer diameter, respectively, the coils are tightly wound with the turn spacing $D \approx a$, and $a$ is wire diameter.

We set the input voltage at $U_s$ = 50 V and the resonance frequency at $f$ = 200 kHz. In Table 1, the TX (RX) resistances of different layers are equal to $R_T$ ($R_R$), and the mutual

inductance of TX and RX in the same layers are equal to $M$. As such, the equalization condition (10) can be simplified as:

$$M_{12} = \frac{R_T}{\omega} + \frac{n\omega M^2}{R_R} \tag{11}$$

Assuming the equalization condition is always satisfied, the relationship between $I_{TX1}$ ($I_{TX2}$), $I_{RX1}$ ($I_{RX2}$) and the RX number $m$, $n$ can be figured according to (7) and (11); the relationship between the output power $P$, the transmission efficiency of $\eta$ and $m$, $n$ can also be figured according to (8) and (9), respectively, where the change in relationship between $P$ and $I_{RX}$ is the same. Given this, only one of the diagrams needs to be made, as shown in Figure 6.

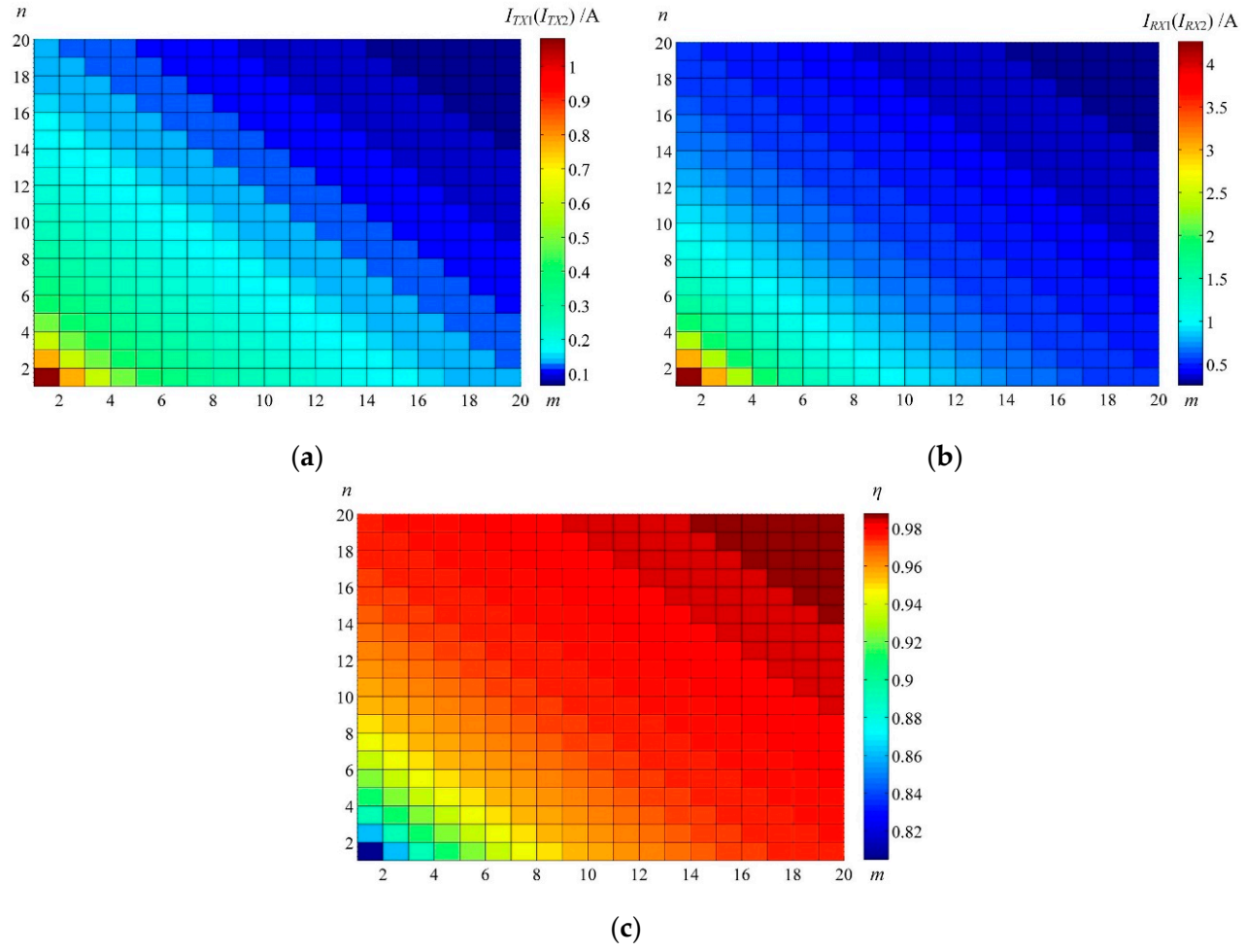


**Figure 6.** (**a**) The relationship between $I_{TX}$ and $m$, $n$. (**b**) The relationship between $I_{RX}$ ($P$) and $m$, $n$. (**c**) The relationship between $\eta$ and $m$, $n$.

We can conclude from Figure 6 that, as $m$ or $n$ increase, $I_{TX}$, $I_{RX}$ ($P$) will decrease accordingly, while $\eta$ will be improved. The number of RX on the first layer $m$ or the second layer $n$ can be limited according to the specific requirements of TX currents, load currents, transmission power, or transmission efficiency.

According to (11) and the parameters listed in Table 1, the relationship between $M_{12}$ and the number of RX on second layer $n$ is shown in Figure 7. $M_{12}$, which satisfies the power equalization condition, is proportional to the number of RX on the second layer $n$. The relationship between $M_{12}$ and $h$ can be obtained using (3) and the parameters in Table 1, as Figure 8 shows.

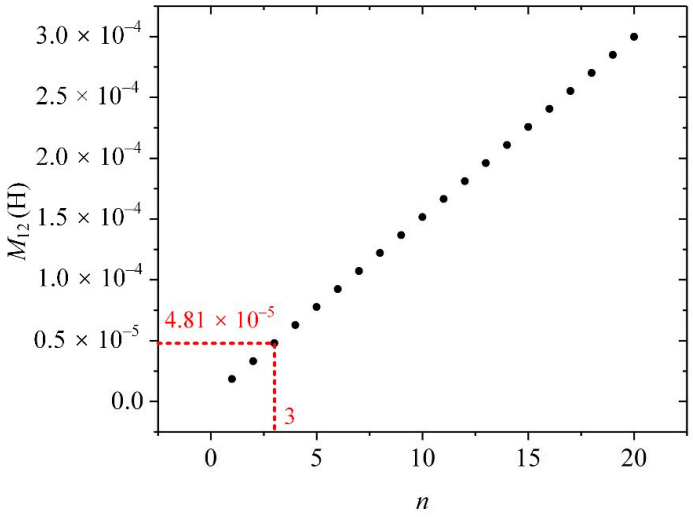


**Figure 7.** The relationship between $M_{12}$ and the number of RX on the second layer $n$, which satisfies the power equalization condition.

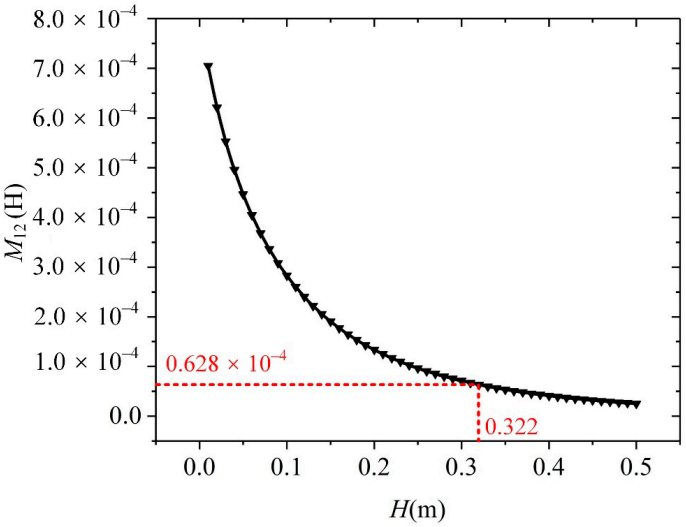


**Figure 8.** The relationship between $M_{12}$ and the transmission distance $h$.

### *3.1. A. Example of the Known h and the Unknown m, n*

Assuming $h$ = 37 cm, the mutual inductance between TX1 and TX2 $M_{12}$ can also be calculated as 48 μH, according to (3). The number of RX on the second layer $n$ should be 3 to meet the equalization condition, as Figure 7 shows.

To achieve a design requirement for mobile phone wireless charging with transmission power $P \geq 19$ W and transfer efficiency $\eta \geq 92\%$, the number of RX on the first layer $m$ can be limited to 3, according to (8) and (9). Then we can calculate that $I_{TX1}$ = 0.415 A, $I_{TX2}$ = 0.415 A, $I_{RX1}$ = 1.632 A, $I_{RX2}$ = 1.632 A.

### *3.2. B. Example of the Known m, n and the Unknown h*

Assuming $m = n = 4$, the mutual inductance between TX1 and TX2 $M_{12}$ can also be calculated as 62.8 μH, according to (3). This means the transmission distance should be 32.2 cm to satisfy the relationship between $M_{12}$ and $h$, as Figure 8 shows. We can calculate that $I_{TX1}$ = 0.317 A, $I_{TX2}$ = 0.317 A, $I_{RX1}$ = 1.247 A, $I_{RX2}$ = 1.247 A.

In practical applications, when transmission distance or load number are unknown, we can satisfy the power equalization condition by adjusting the TX resistance with an impedance matching network. If the TX coil is offset (angular or horizontal), the mutual inductance between the TXs will be changed according to (3). Correspondingly, the

parameters in (11) must be adjusted to meet the power equalization condition. The implementation flowchart of adjusting the internal resistance value of transmitter coil loop and relay transmitter coil loop, according to different load numbers and transmission distances, is shown in Figure 9.

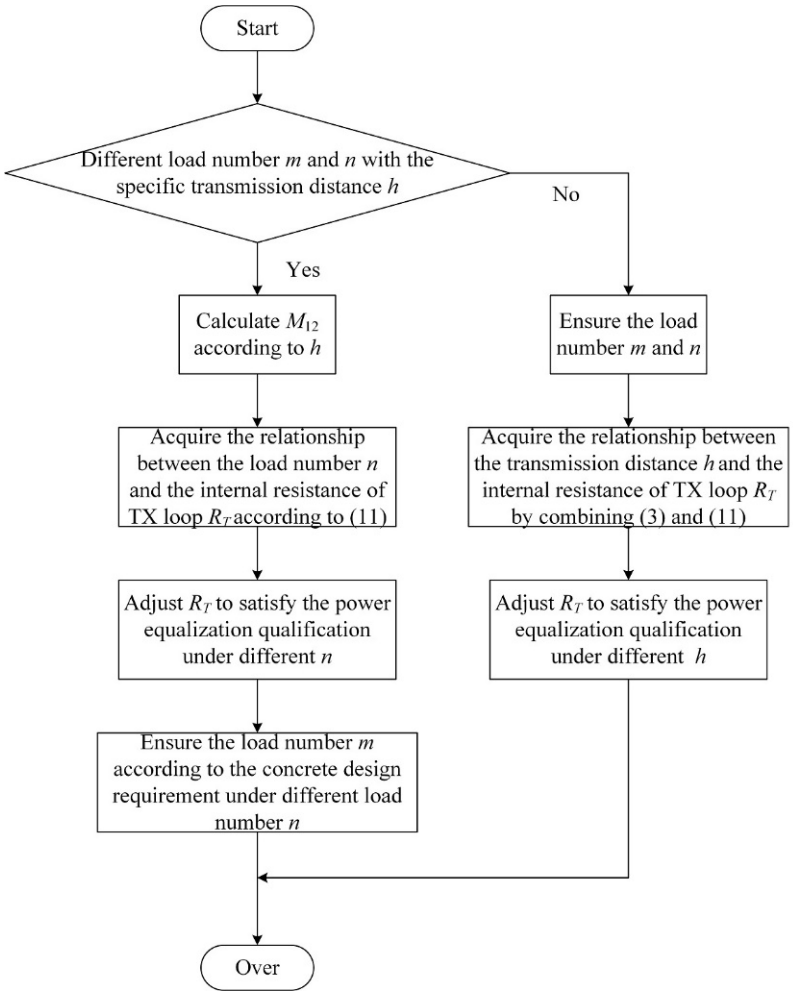


**Figure 9.** Flow chart of the adjustment of $R_T$ according to different transmission distances and load numbers.

## 4. Electromagnetic Field Simulation

Using the parameters in Table 1, we can set the operating frequency $f$ to 200 kHz and the transmission distance $h$ to 32.2 cm. Taking the worst situation into consideration, the input voltage $U_s$ is raised to 100 V, which will cause the currents in TX1 and TX2 to increase to 0.63 A, and the currents in all RXs to increase to 2.49 A. The simulation model is shown in Figure 10a, and the entire H-field intensity distribution is provided in Figure 10b.

To visualize the magnetic field distribution around the WPT system, we study the H-field strength along two lines in Figure 10b. The simulation results are shown in Figure 11, where "I" represents the H-field intensity distribution in the horizontal direction, "II" represents that in vertical direction, while "III" represents the reference level according to ICNIRP-2018 [21].

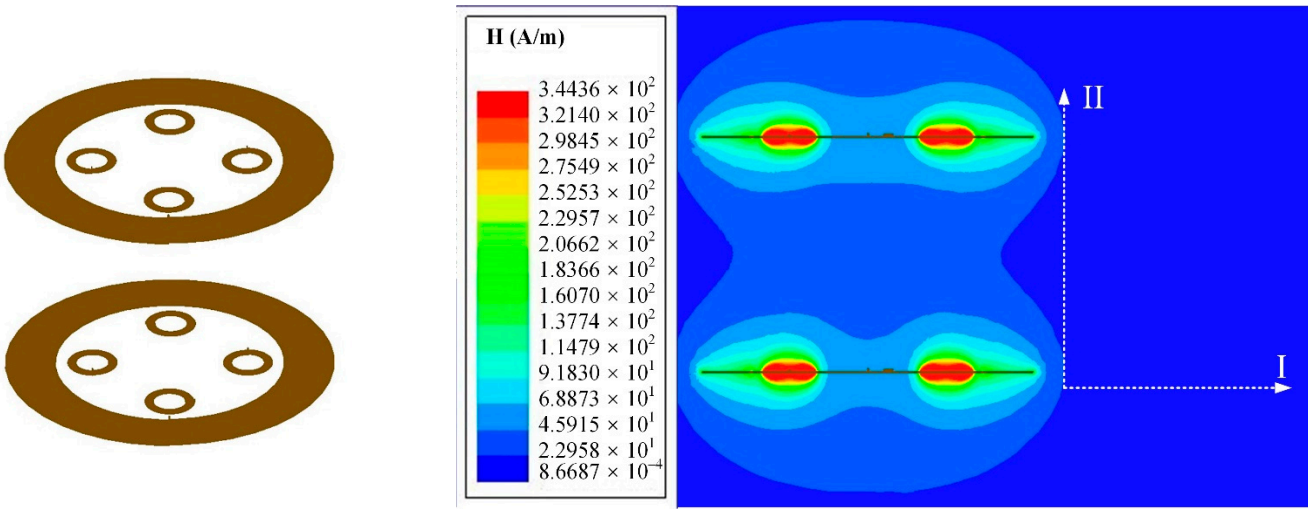


**Figure 10.** (**a**) The simulation model of the proposed structure; (**b**) the H-field strength of the simulation model from the front view.

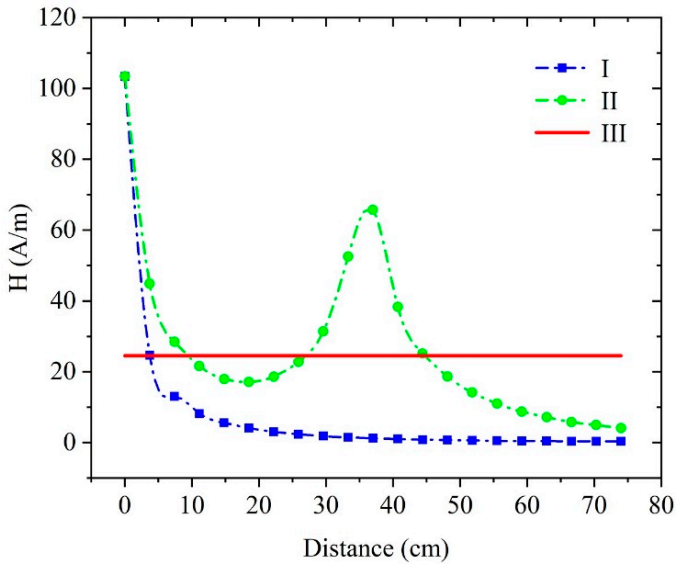


**Figure 11.** H-field strength along lines I, II and reference level III.

The H-field strength along line "II" clearly shows a strong magnetic field distribution to RX and TX. However, the H-field strength along line "I" (4 cm away from the TX edge) is always below the reference level, which reflects the fact that the WPT system does no harm to people nearby, even in a worst-case scenario. Therefore, the WPT system exhibits a good performance in an electromagnetic environment.

## 5. Experimental Verification

As shown in Figure 12, an experimental prototype was established, according to the parameters in Table 1, to verify the feasibility of the proposed structure and the correctness of the power equalization condition. The TX side was connected to a high-frequency AC power supply by a phase-shifted, full-bridge inverter; the working frequency was 200 kHz and the actual input voltage of $U_S$ was 50 V. The compensation capacitor value was calculated according to the resonance conditions and operating frequency, and, at the same time, a parallel connection method was used to reduce voltage on the capacitor. The RX side was connected to a lamp, so it was not rectified, but directly output a high-frequency alternating current. For convenience, TX1 and TX2 were completely the same, as well as

RX1 and RX2. Two oscilloscopes were used to measure and display the voltage and current parameters of the system. One was used to measure the drive voltage and input voltage, whereas the other was used to measure the current of TX1 and TX2.

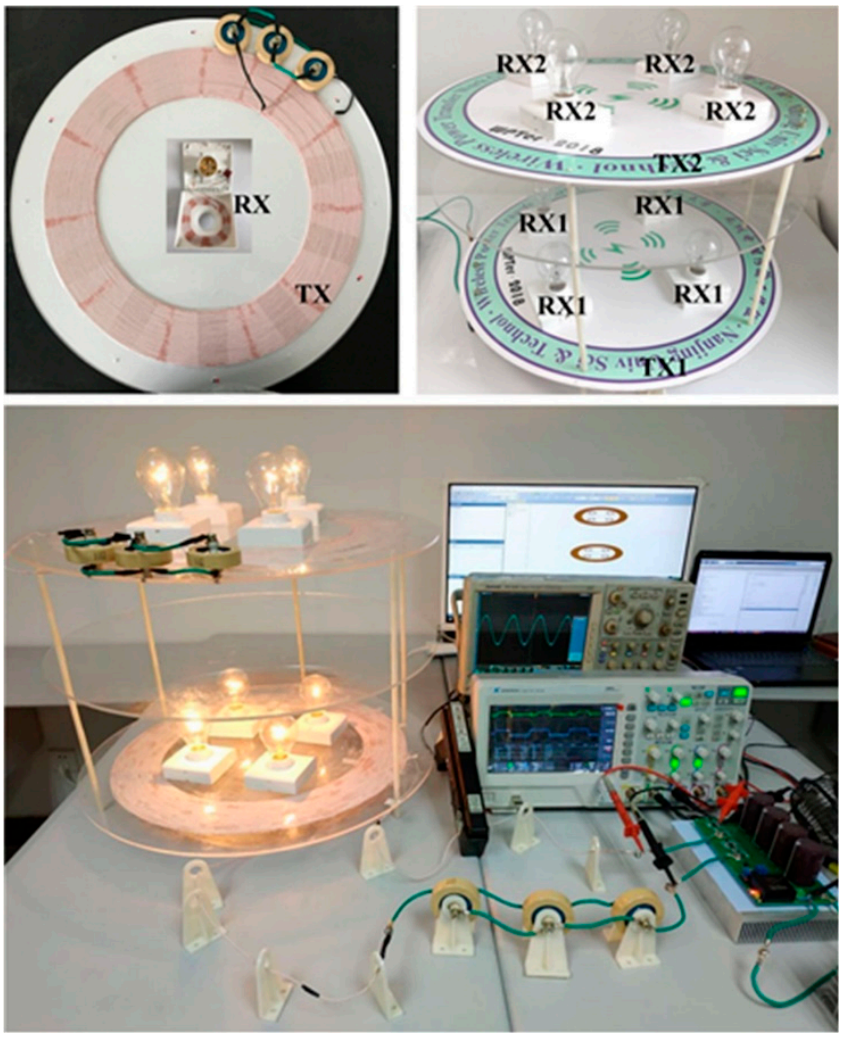


**Figure 12.** Experimental prototype, including high frequency power supply, TX and RX.

When $h$ = 37 cm and $m = n = 3$, the currents in the TX1, TX2, RX1 and RX2 loops would theoretically be 0.415 A, 0.415 A, 1.632 A and 1.632 A, respectively. When $h$ = 32.2 cm and $m = n = 4$, the currents in TX1, TX2, RX1 and RX2 loops were anticipated to be 0.317 A, 0.317 A, 1.247 A and 1.247 A, respectively. Due to the harsher conditions considered in the simulation ($U_S$ increased to 100 V), the system electromagnetic environment was further improved in the experiment.

### *5.1. A. Experiment with the Known h and the Unknown m, n*

When the transmission distance between TX1 and TX2 is $h$ = 37 cm, the number of RX on the first layer $m$ and the second layer $n$ should be 3, and the currents $I_{TX1}$, $I_{TX2}$ should equal 0.415 A, according to the analysis in Section 3.1. Figure 13a shows the input voltage as $U_s$ = 49.2 V, and Figure 13b shows the currents in the transmitter coil loop as $I_{TX1}$ = 0.55 A and the relay transmitter coil loop as $I_{TX2}$ = 0.445 A.

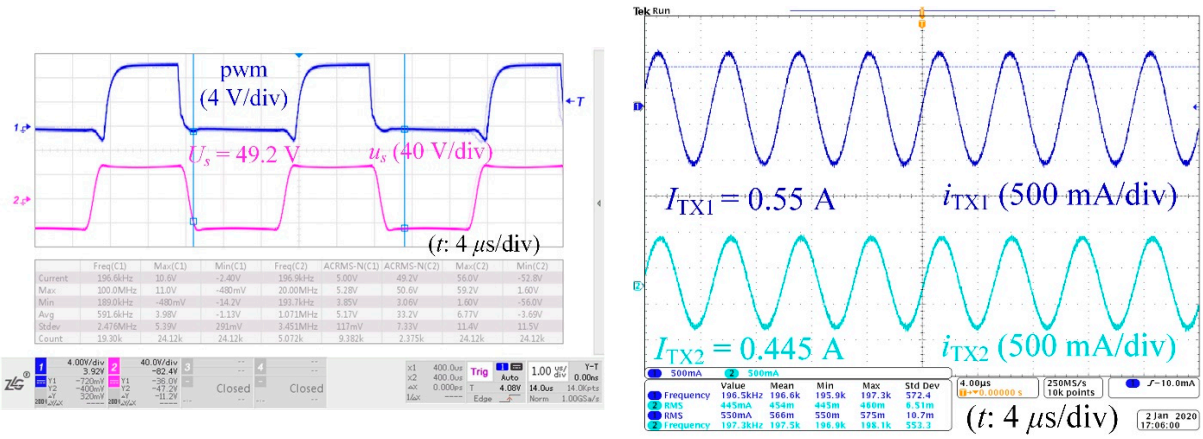


(**a**) (**b**)

**Figure 13.** As $h$ = 37 cm, $m$ = $n$ = 3, (**a**) the input voltage $Us$; (**b**) the currents in the TX1 and TX2.

Both $I_{TX1}$ and $I_{TX2}$ increased slightly when compared with the theoretical values, which may be due to the nonlinear resistance of incandescent lamps connected to each receiver coil. The internal resistance of the incandescent lamp increased with the rising temperature, so the actual value of $R_R$ was larger than the simulation result, which would cause $I_{TX1}$ and $I_{TX2}$ to increase. As we can observe in Figure 13b, there was also a difference between $I_{TX1}$ and $I_{TX2}$. In fact, $I_{TX1}$ equals $I_{TX2}$ to a certain extent; that is, $I_{RX1}$ was approximately equal to $I_{RX2}$, which could prove the validity of the proposed structure and the correctness of the power equalization condition.

We also kept $h$ = 37 cm and added the number of the RX $m$ and $n$ to 4. Figure 14a shows the input voltage as $U_s$ = 50.4 V, and Figure 14b shows $I_{TX1}$ = 0.693 A and $I_{TX2}$ = 0.466 A. The difference between $I_{TX1}$ and $I_{TX2}$ will grow larger as $m$ and $n$ increase further, which means the power received in each load starts to become unequal.

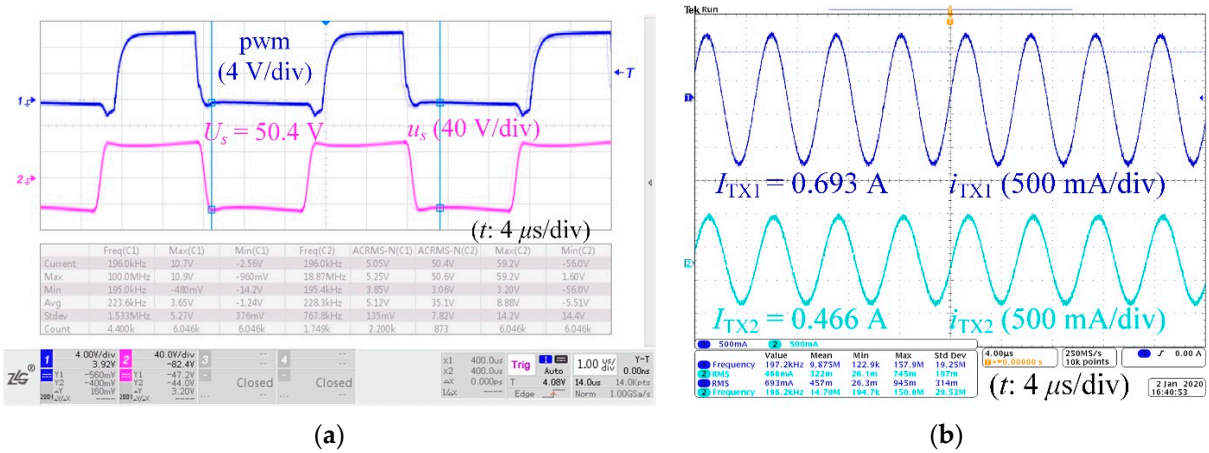


(**a**) (**b**)

**Figure 14.** As $h$ = 37 cm, $m$ = $n$ = 4, (**a**) the input voltage $Us$; (**b**) the currents in the TX1 and TX2.

### *5.2. B. Experiment with the Known m, n and the Unknown h*

When the number of RX on the first and second layers $m$ = $n$ = 4 kept the transmission distance as $h$ = 32.2 cm, the current received in each load was 0.317 A, according to the analysis in Section 3.2. Figure 15a shows the input voltage as $U_s$ = 49.8 V, and Figure 15b shows the currents in the transmitter coil loop as $I_{TX1}$ = 0.498 A and the relay transmitter coil loop as $I_{TX2}$ = 0.42 A. When comparing the measured root mean square (RMS) values with the calculated values of $I_{TX1}$ = $I_{TX2}$ = 0.317 A, there is a difference between these two

sets of data due to the existence of incandescent lamps. $I_{TX1}$ equals $I_{TX2,}$ to a certain extent, so $I_{RX1}$ is approximately equal to $I_{RX2}$.

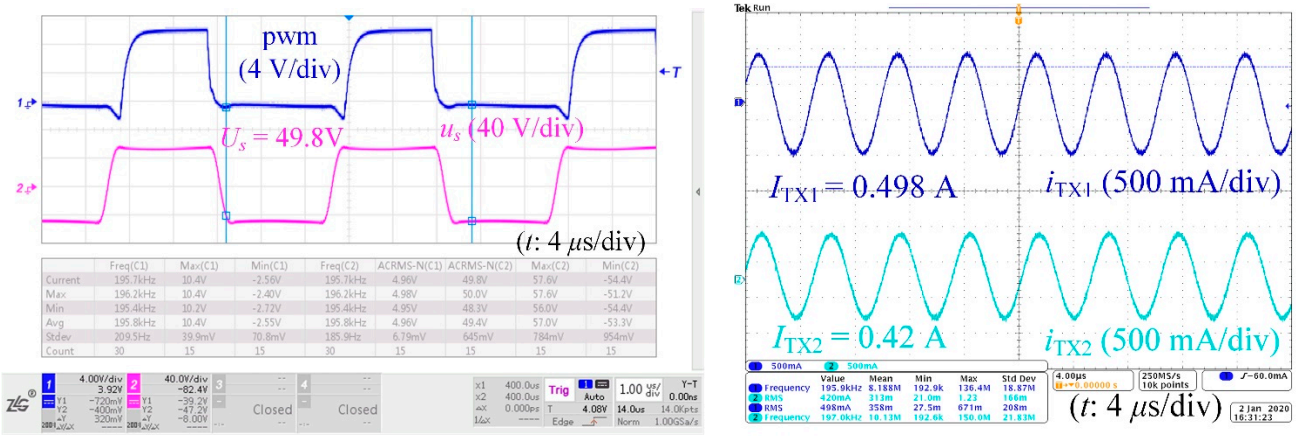


(**a**) (**b**)

**Figure 15.** As $h$ = 32.2 cm, $m = n$ = 4, (**a**) the input voltage $Us$; (**b**) the currents in the TX1 and TX2.

We also kept $m = n$ = 4 and increased $H$ to 37 cm. The input voltage $U_s$, the currents in the transmitter coil loop $I_{TX1}$, and the relay transmitter coil loop $I_{TX2}$ are shown in Figure 14 above. The difference between $I_{TX1}$ and $I_{TX2}$ in Figure 15 is much less than that in Figure 14, which could also demonstrate the power equalization phenomenon.

Table 2 shows the comparison of the theoretical and experimental values of TX current at different transmission distances and RX numbers. The power difference rate can be defined as follows:

$$D_P = \frac{P_{\max} - P_{\min}}{P_{\max}} = \frac{I_{\max} - I_{\min}}{I_{\max}} \tag{12}$$

**Table 2.** Comparison of theoretical and experimental values.

| Parameter | | Case 1: $h$ = 37 cm, $m = n$ = 3 | Case 2: $h$ = 37 cm, $m = n$ = 4 | Case 3: $h$ = 32.2 cm, $m = n$ = 4 |
|---|---|---|---|---|
| Theory | $I_{TX1}$ | 0.415 A | 0.4 A | 0.317 A |
| | $I_{TX2}$ | 0.415 A | 0.318 A | 0.317 A |
| Experiment | $I_{TX1}$ | 0.55 A | 0.693 A | 0.498 A |
| | $I_{TX2}$ | 0.445 A | 0.466 A | 0.42 A |
| Power different rate | | 19.1% | 32.8% | 15.7% |

The experimental and theoretical results are different, but the error is within the allowable range. On the one hand, the measured value of the coil's internal resistance is not accurate. On the other hand, it is caused by the winding error of the coil. The experimental results show that the power difference rate under the power equalization condition is smaller, which verifies the effectiveness of power equalization.

## 6. Conclusions

In this paper, a new type of WPT system, with multiple receivers in different layers, was proposed for application scenarios, such as electric vehicles in multistorey garages, which can balance the received power by adjusting the circuit resistance of the transmitter. The major contributions of this paper are as follows.

(1) A new stereo multireceiver WPT system is proposed, and the power equalization condition is derived.

(2) A method for adjusting the resistance of transmitter loops is proposed, which can satisfy the power equalization condition under different transmission distances or load numbers, without the need for redesigning coils or adding additional control circuits.

Experimental results show that, under the condition of satisfying power equalization, the power differential rate of the system is lower, which verifies the feasibility of the method. At the same time, the simulation results show that the H-field intensity around the working system is within the limit level of the ICNIRP-2018 standard, which proves that the proposed structure can also exhibit good performance in an electromagnetic environment. This study is of great value to the application of wireless charging systems with multiple identical loads.

**Author Contributions:** F.W. conceived and designed the study, and this work was performed under the advice of, and regular feedback from, him. B.S. was responsible for the models and simulations. X.C. wrote the article, and was responsible for the experiments and data analysis. All authors have read and agreed to the published version of the manuscript.

**Funding:** This work was Funded by China Postdoctoral Science Foundation (2020M671498), the Basic Research Program of Jiangsu Province (BK20180485), the Fundamental Research Funds for the Central Universities (30919011241), the Jiangsu Planned Projects for Postdoctoral Research Funds (2020Z374), and the Science and Technology Project of State Grid Jiangsu Electric Power Co., Ltd. (J2020135, SGJSJX00BGJS2002373).

**Conflicts of Interest:** The authors declare no conflict of interest. The funders had no role in the design of the study; in the collection, analyses, or interpretation of data; in the writing of the manuscript, or in the decision to publish the results.

## References

1. Kurs, A.; Karalis, A.; Moffatt, R. Wireless power transfer via strongly coupled magnetic resonances. *Science* **2007**, *317*, 83–86. [CrossRef] [PubMed]
2. Karalis, A.; Joannopoulos, J.D.; Soljacic, M. Efficient wireless non-radiative mid-range energy transfer. *Ann. Phys.* **2008**, *323*, 34–48. [CrossRef]
3. Agarwal, K.; Jegadeesan, R.; Guo, Y. Wireless Power Transfer Strategies for Implantable Bioelectronics. *IEEE Rev. Biomed. Eng.* **2017**, *10*, 136–161. [CrossRef] [PubMed]
4. Patil, D.; McDonough, M.K.; Miller, J.M. Wireless Power Transfer for Vehicular Applications: Overview and Challenges. *IEEE Trans. Transp. Electrif.* **2018**, *4*, 3–37. [CrossRef]
5. Nguyen, V.T.; Kang, S.H.; Choi, J.H. Magnetic resonance wireless power transfer using three-coil system with single planar receiver for laptop applications. *IEEE Trans. Consum. Electron.* **2015**, *61*, 160–166.
6. Shinohara, N. Trends in Wireless Power Transfer: WPT Technology for Energy Harvesting, Mllimeter-Wave/THz Rectennas, MIMO-WPT, and Advances in Near-Field WPT Applications. *IEEE Microw. Mag.* **2021**, *22*, 46–59. [CrossRef]
7. Liu, F.; Yang, Y.; Ding, Z. A Multifrequency Superposition Methodology to Achieve High Efficiency and Targeted Power Distribution for a Multiload MCR WPT System. *IEEE Trans. Power Electron.* **2018**, *33*, 9005–9016. [CrossRef]
8. Bu, Y.; Mizuno, T.; Fujisawa, H. Proposal of a Wireless Power Transfer Technique for Low-Power Multireceiver Applications. *IEEE Trans. Magn.* **2015**, *51*, 1–4. [CrossRef]
9. Song, J.; Liu, M.; Ma, C. Efficiency optimization and power distribution design of a megahertz multi-receiver wireless power transfer system. In Proceedings of the 2017 IEEE PELS Workshop on Emerging Technologies: Wireless Power Transfer (WoW), Chongqing, China, 21–22 May 2017; pp. 54–58.
10. Fu, M.; Zhao, C.; Song, J. A Low-Cost Voltage Equalizer Based on Wireless Power Transfer and a Voltage Multiplier. *IEEE Trans. Ind. Electron.* **2018**, *65*, 5487–5496. [CrossRef]
11. Liu, M.; Fu, M.; Wang, Y.; Ma, C. Battery Cell Equalization via Megahertz Multiple-Receiver Wireless Power Transfer. *IEEE Trans. Power Electron.* **2018**, *33*, 4135–4144. [CrossRef]
12. Bu, Y.; Mukhopadhyay, S.C. Equalization Method of the Wireless Power Transfer in an Electronic Shelf Label Power Supply System. *IEEE Trans. Magn.* **2017**, *53*, 1–5.
13. Zhong, W.; Hui, S.Y.R. Auxiliary Circuits for Power Flow Control in Multifrequency Wireless Power Transfer Systems with Multiple Receivers. *IEEE Trans. Power Electron.* **2015**, *30*, 5902–5910. [CrossRef]
14. Shang, Y.; Xia, B.; Lu, F.; Zhang, C.; Cui, N.; Mi, C.C. A switched coupling-capacitor equalizer for series-connected battery strings. *IEEE Trans. Power Electron.* **2017**, *32*, 7694–7706. [CrossRef]
15. Shang, Y.; Xia, B.; Zhang, C.; Cui, N.; Yang, J.; Mi, C.C. An automatic equalizer based on forward-flyback converter for series-connected battery strings. *IEEE Trans. Ind. Electron.* **2017**, *64*, 5380–5391. [CrossRef]

16. Liu, Z.; Chen, Z.; Li, J. A Shape-Reconfigurable Modularized Wireless Power Transfer Array System for Multipurpose Wireless Charging Applications. *IEEE Trans. Antennas Propag.* **2018**, *66*, 4252–4259. [CrossRef]
17. Gallardo-Lozano, J.; Romero-Cadaval, E.; Milanes-Montero, M.I. Battery equalization active methods. *J. Power Sources* **2014**, *246*, 934–949. [CrossRef]
18. SAE International. *SAE J2954: Wireless Power Transfer for Light-Duty Plug-in/Electric Vehicles and Alignment Methodology*; SAE International: Warrendale, PA, USA, 2019.
19. Jeong, N.S.; Carobolante, F. Wireless Charging of a Metal-Body Device. *IEEE Trans. Microw. Theory Tech.* **2017**, *65*, 1077–1086. [CrossRef]
20. ICNIRP. Guidelines for limiting exposure to time-varying electric, magnetic, and electromagnetic fields (up to 300 GHz). *Health Phys.* **2010**, *99*, 818–836. [CrossRef] [PubMed]
21. Stam, R. Progress report: ICNIRP Statement on non-ionizing radiation for cosmetic purposes. In Proceedings of the 2018 EMF-Med 1st World Conference on Biomedical Applications of Electromagnetic Fields (EMF-Med), Split, Croatia, 10–13 September 2018; pp. 1–2.
22. IEEE Std C95.3-2002—IEEE Recommended Practice for Measurements and Computations of Radio Frequency Electromagnetic Fields with Respect to Human Exposure to Such Fields, 100 kHz–300 GHz. Revision of IEEE Std C95.3-1991. 2003. Available online: https://ieeexplore.ieee.org/document/8329043 (accessed on 1 March 2021).
23. IEEE Std C95.1-2005—IEEE Standard for Safety Levels with Respect to Human Exposure to Radiofrequency Electromagnetic Fields, 3 kHz to 300 GHz. Revision of IEEE Std C95.1-1991. 2006. Available online: https://ieeexplore.ieee.org/document/1626482 (accessed on 1 March 2021).